# Azobenzene-Derivated *tris*–*β*–Diketonates Lanthanide Complexes: Reversible *trans*–to–*cis* Photoisomerization in Solution and Solid State

Li-Rong Lin,*[,†] Xuan Wang,[†] Gao-Ning Wei,[†] Hui-Hui Tang,[†] Hui Zhang,[†] Li-Hua Ma*[,‡]

[†] *Department of Chemistry, College of Chemistry and Chemical Engineering, Xiamen University, Xiamen, 361005, P. R. China*

[‡] *Department of Chemistry, School of Science and Computer Engineer, University of Houston at Clear Lake, 2700 BAY AREA BLVD, Houston, TX, 77058*

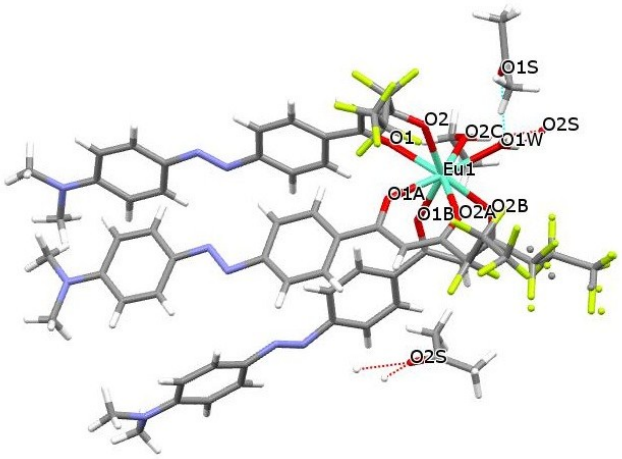


Figure S1. Crystal structure of Eu(**LB**)$_3$($CH_3CH_2OH$)($H_2O$). Selected bonds distances (Å) and angles (°) : Eu1–O1B 2.315(4), Eu1–O2A 2.333(5), Eu1– O2 2.360(4), Eu1– O1A 2.364(4) , Eu1–O1 2.369(4), Eu1–O2B 2.408(4), Eu1–O1W 2.427(5), Eu1–O2C 2.462(4); O1B–Eu1–O2A 95.88(17), O1B –Eu1–O2 141.63(14), O1B –Eu1–O1A 73.67(16), O2A–Eu1–O1A 69.47(14), O1B–Eu1–O1W 142.86(18), O2A–Eu1–O1W 82.10(18), O2–Eu1–O1W 74.99(16), O1B–Eu1–O2C 91.02(17).

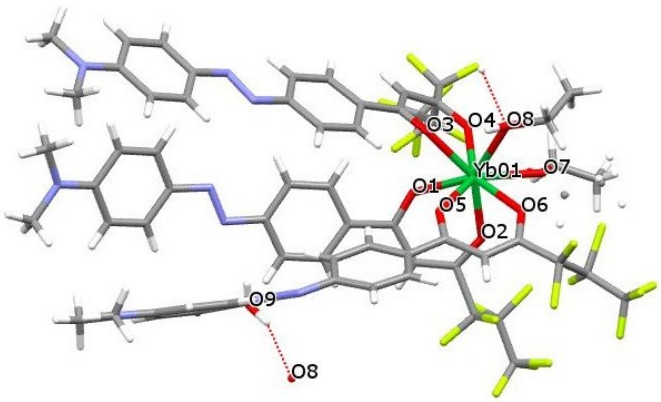


Figure S2. Crystal structure of Yb(**LB**)$_3$ ($CH_3CH_2OH$)$_2$. Selected bonds distances (Å) and angles (°) : Yb01–O5 2.229(8), Yb01–O4 2.271(8), Yb01–O3 2.280(6),Yb01–O2 2.279(8), Yb01–O6 2.281(8), Yb01–O1 2.304(8), Yb01–O8 2.344(9), Yb01–O7 2.252(10); O1–Yb01–O7 135.6(6), O2–Yb01–O8 145.7(3), O3–Yb01–O8 69.4(3), O4–Yb01–O2 108.3(3), O5–Yb01–O4 142.6(2), O6–Yb01–O1 136.6(2), O3–Yb01–O6 125.4(3) , O5–Yb01–O8 102.1(4).

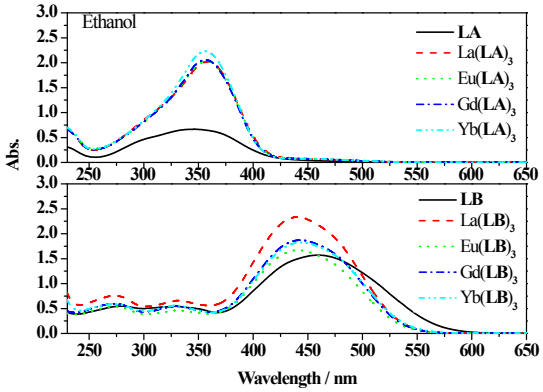


Figure S3. UV–Vis absorption spectra of **LA, LA–**Ln(III) and **LB, LB–**Ln(III) ($5.0 \times 10^{-5}$ mol $L^{-1}$) in ethanol solutions.

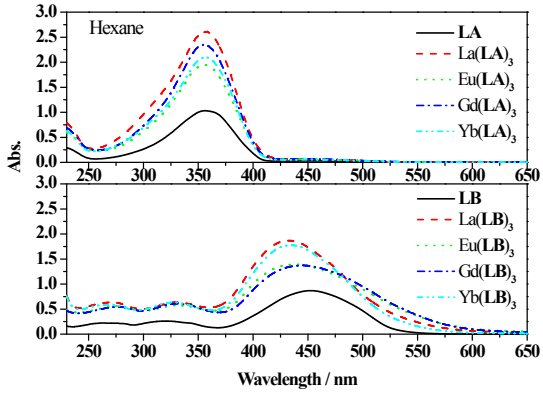


Figure S4. UV–Vis absorption spectra of **LA, LA–**Ln(III) and **LB, LA–**Ln(III) ($5.0 \times 10^{-5}$ mol $L^{-1}$) in hexane solutions.

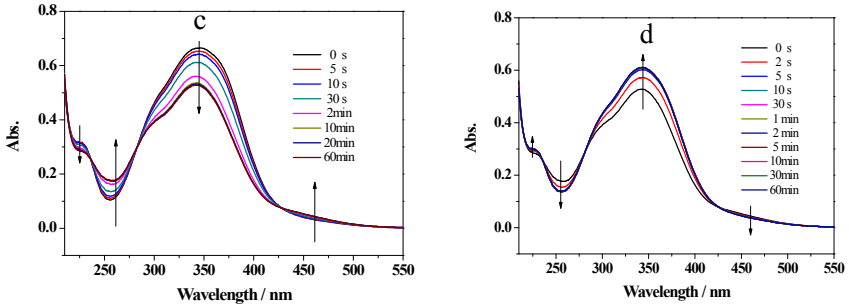


Figure S5. UV–Vis spectral change of **LA** in ethanol ($2.0\times 10^{-5}$ mol $L^{-1}$) solution upon irradiation at 365 nm (c) and recoverable irradiation at 450 nm (d) as a function of time.

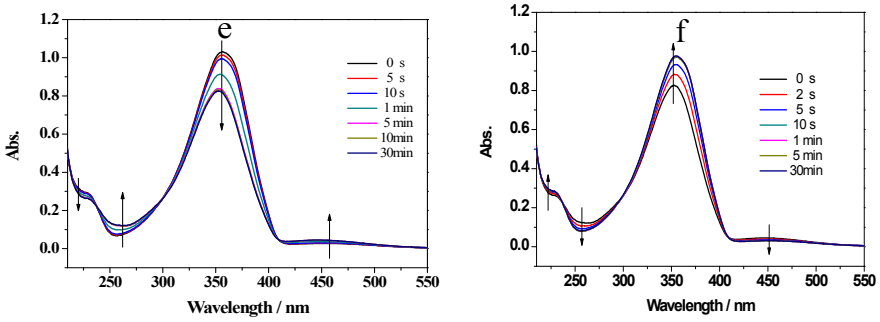


Figure S6. UV–Vis spectral change of **LA** in hexane ($2.0\times 10^{-5}$ mol $L^{-1}$) solution upon irradiation at 365 nm (e) and recoverable irradiation at 450 nm (f) as a function of time.

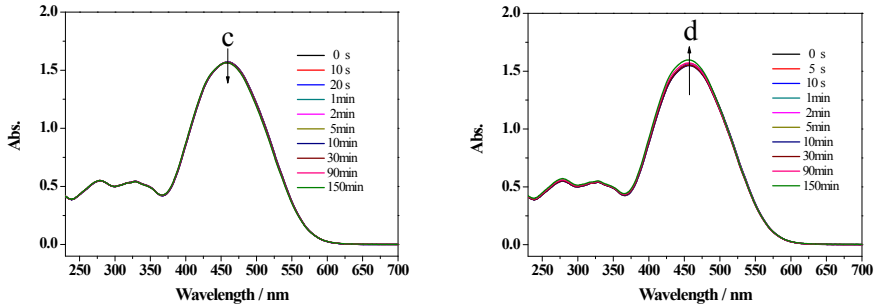


Figure S7. UV–Vis spectral change of **LB** in ethanol ($2.0\times 10^{-5}$mol $L^{-1}$) solution upon irradiation at 365 nm (c) and recoverable irradiation at 450 nm (d) as a function of time.

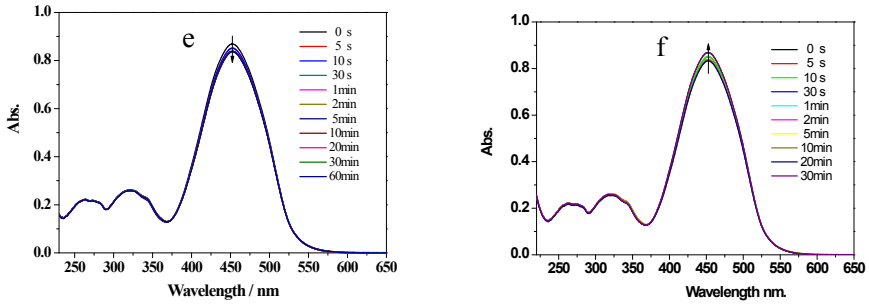


Figure S8. UV–Vis spectral change of **LB** in hexane ($2.0\times 10^{-5}$mol $L^{-1}$) solution upon irradiation at 365 nm (e) and recoverable irradiation at 450 nm (f) as a function of time.

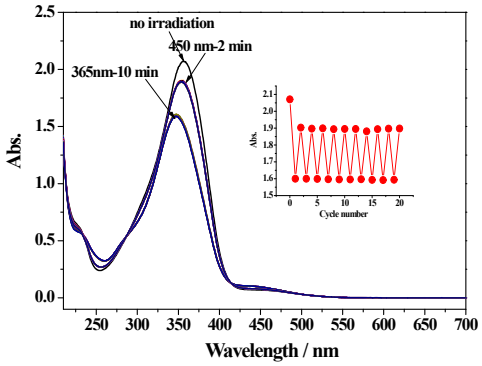


Figure S9. Absorption spectra of Yb(**LA**)$_3$ in acetonitrile solution under no irradiation, and in the photostationary states after alternating irradiation at $\lambda = 365$ and $\lambda = 450$ nm in repeating switching cycles (Inset: reversible change of absorption intensity at 358 nm).

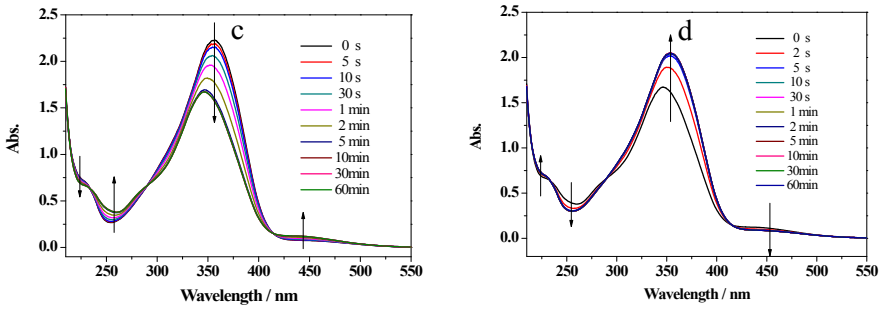


Figure S10. UV–Vis spectral change of Yb(**LA**)$_3$ in ethanol ($2.0\times 10^{-5}$mol L$^{-1}$) solution upon irradiation at 365 nm (c) and recoverable irradiation at 450 nm (d) as a function of time.

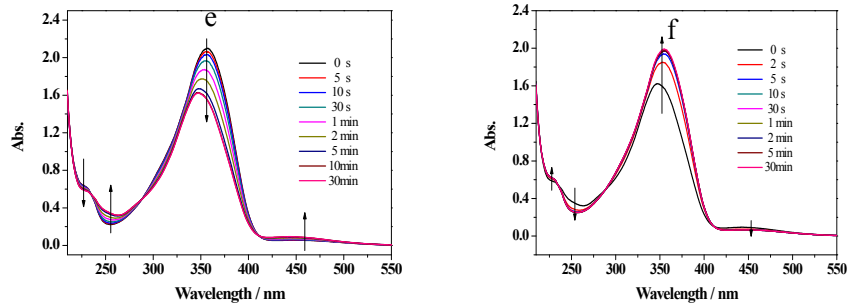


Figure S11. UV–Vis spectral change of Yb(**LA**)$_3$ in hexane ($2.0\times 10^{-5}$mol L$^{-1}$) solution upon irradiation at 365 nm (e) and recoverable irradiation at 450 nm (f) as a function of time.

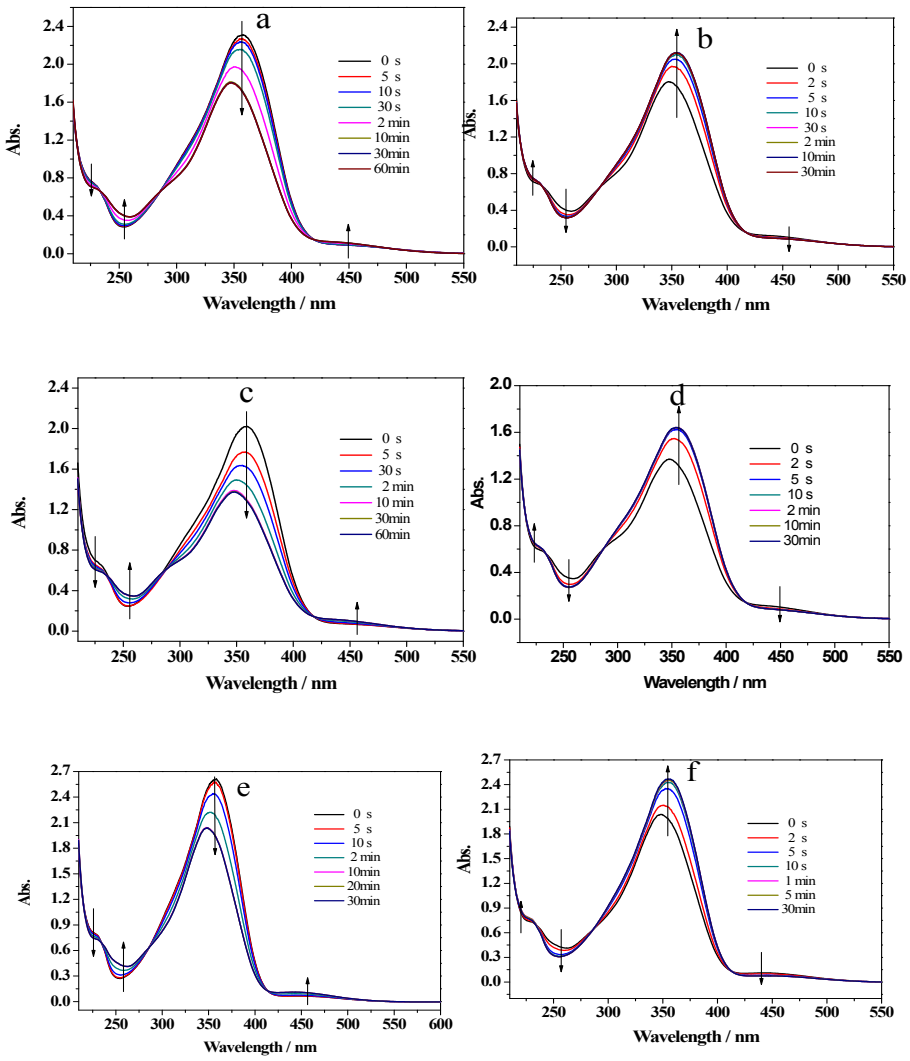


Figure S12. UV–Vis spectral change of La(**LA**)$_3$ in acetonitrile(a, b), ethanol (c, d) and hexane (e, f) ($2.0\times 10^{-5}$mol $L^{-1}$) solutions upon irradiation at 365 nm (a, c, e) and recoverable irradiation at 450 nm (b, d, f) as a function of time.

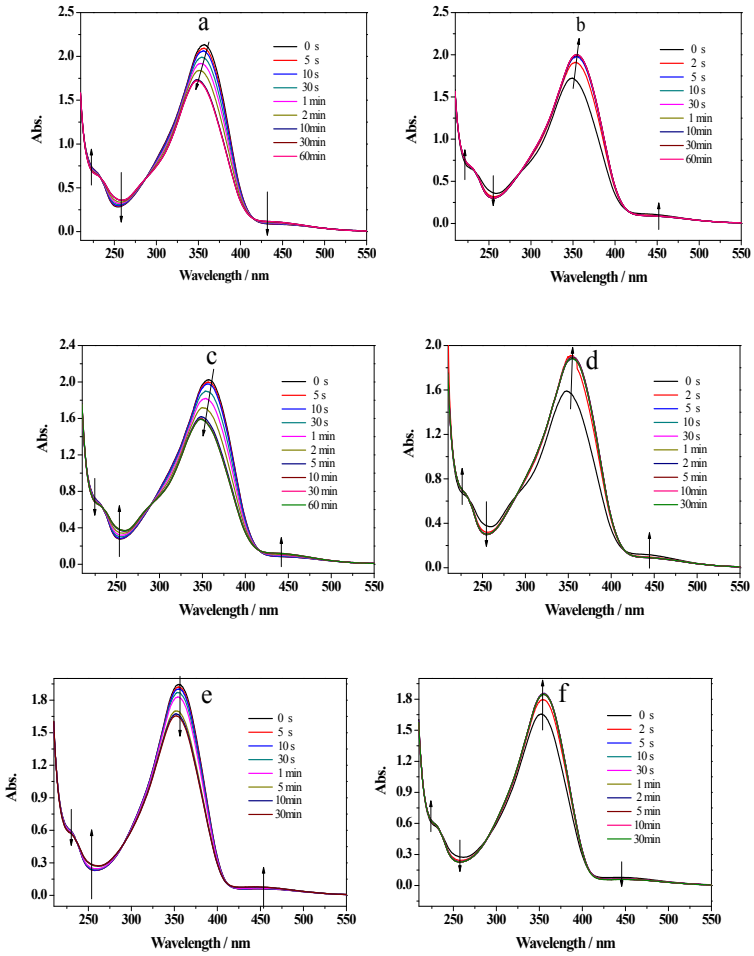


Figure S13. UV–Vis spectral change of Eu(**LA**)$_3$ in acetonitrile(a, b), ethanol (c, d) and hexane (e, f) ($2.0\times 10^{-5}$mol $L^{-1}$) solutions upon irradiation at 365 nm (a, c, e) and recoverable irradiation at 450 nm (b, d, f) as a function of time.

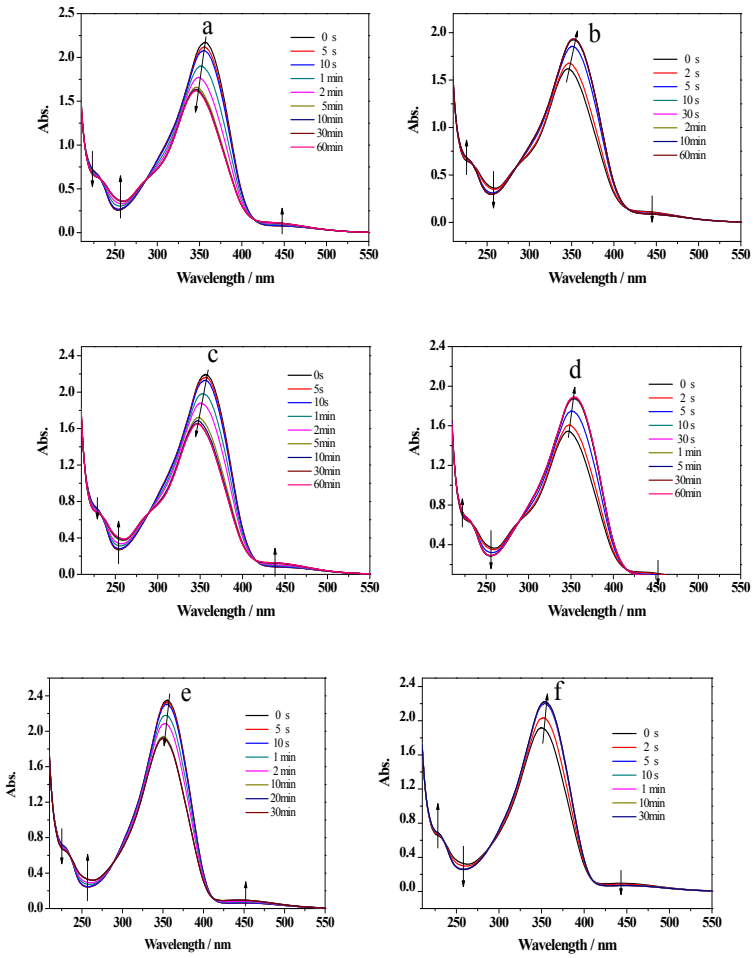


Figure S14. UV–Vis spectral change of Gd(**LA**)$_3$ in acetonitrile(a, b), ethanol (c, d) and hexane (e, f) ($2.0\times10^{-5}$mol $L^{-1}$) solutions upon irradiation at 365 nm (a, c, e) and recoverable irradiation at 450 nm (b, d, f) as a function of time.

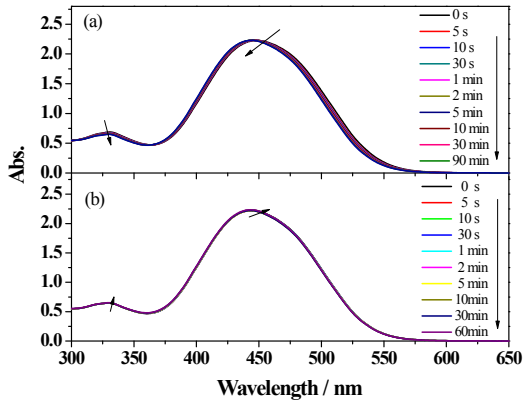


Figure S15. UV–Vis spectral change of Yb(**LB**)$_3$ in acetonitrile ($2.0\times10^{-5}$ mol $L^{-1}$) upon irradiation at 365 nm (a) and recoverable irradiation at 450 nm (b) as a function of time.

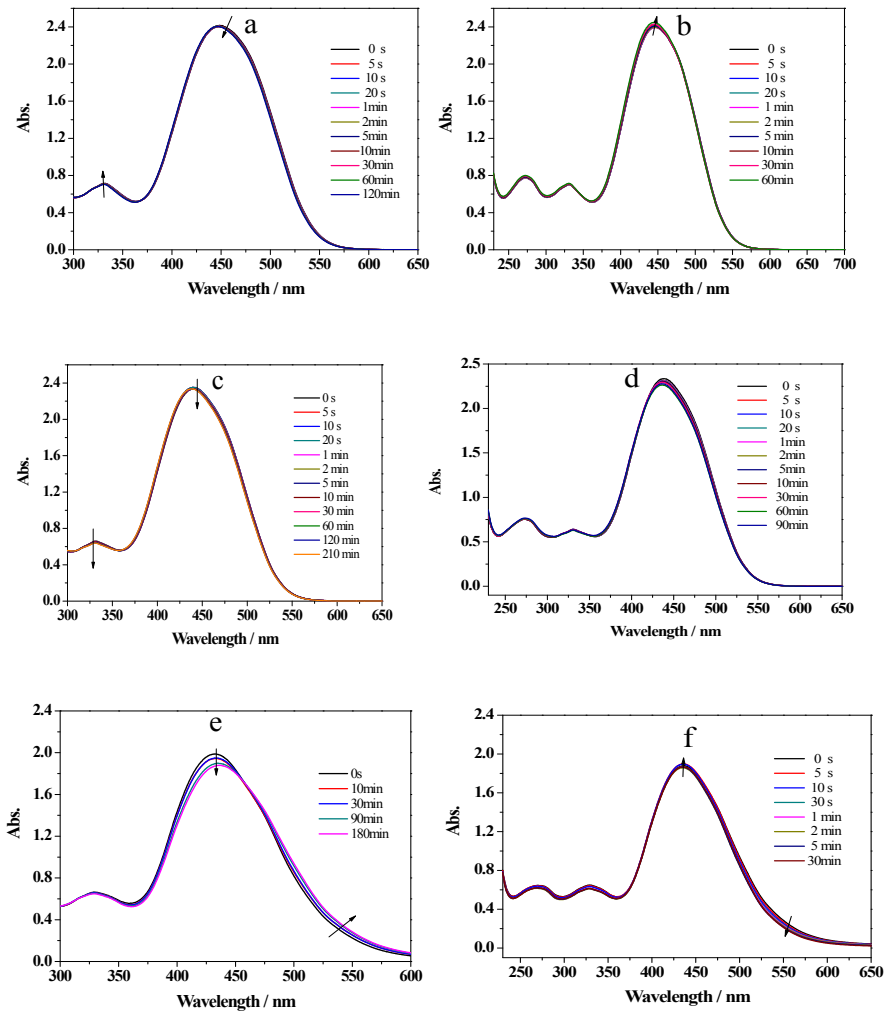


Figure S16. UV–Vis spectral change of La(**LB**)$_3$ in acetonitrile (a, b), ethanol (c, d) and hexane (e, f) ($2.0\times 10^{-5}$mol $L^{-1}$) solutions upon irradiation at 365 nm (a, c, e) and recoverable irradiation at 450 nm (b, d, f) as a function of time.

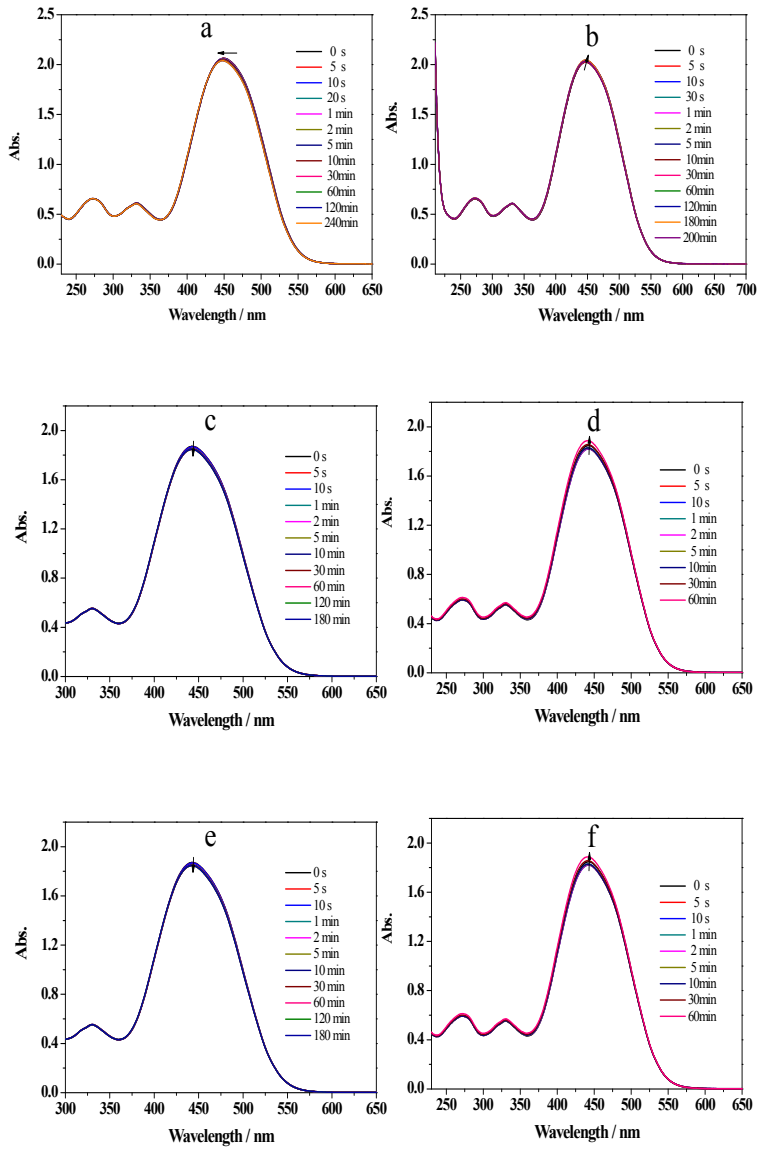


Figure S17. UV–Vis spectral change of Eu(**LB**)$_3$ in acetonitrile (a, b), ethanol (c, d) and hexane (e, f) ($2.0\times 10^{-5}$mol $L^{-1}$) solutions upon irradiation at 365 nm (a, c, e) and recoverable irradiation at 450 nm (b, d, f) as a function of time.

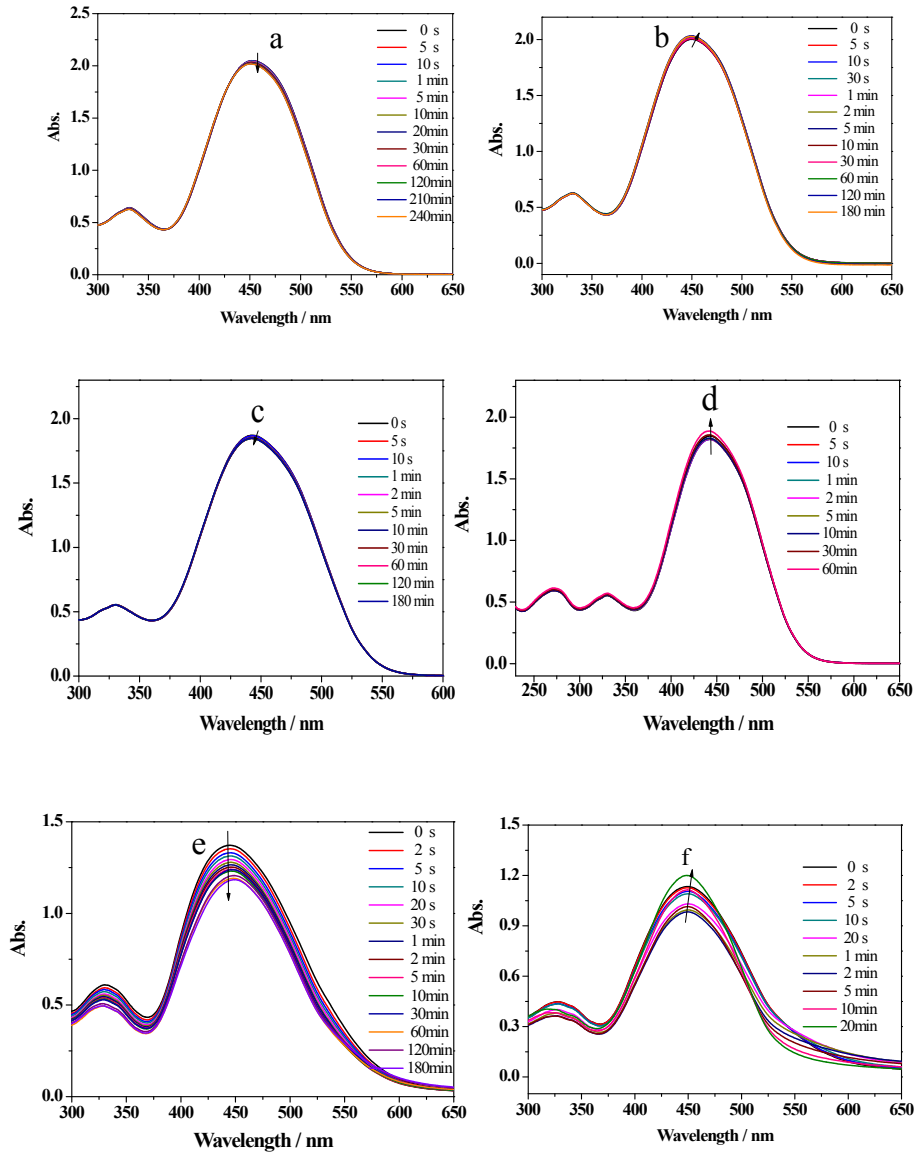


Figure S18. UV–Vis spectral change of Gd(**LB**)$_3$ in acetonitrile (a, b), ethanol (c, d) and hexane (e, f) ($2.0\times 10^{-5}$mol $L^{-1}$) solutions upon irradiation at 365 nm (a, c, e) and recoverable irradiation at 450 nm (b, d, f) as a function of time.

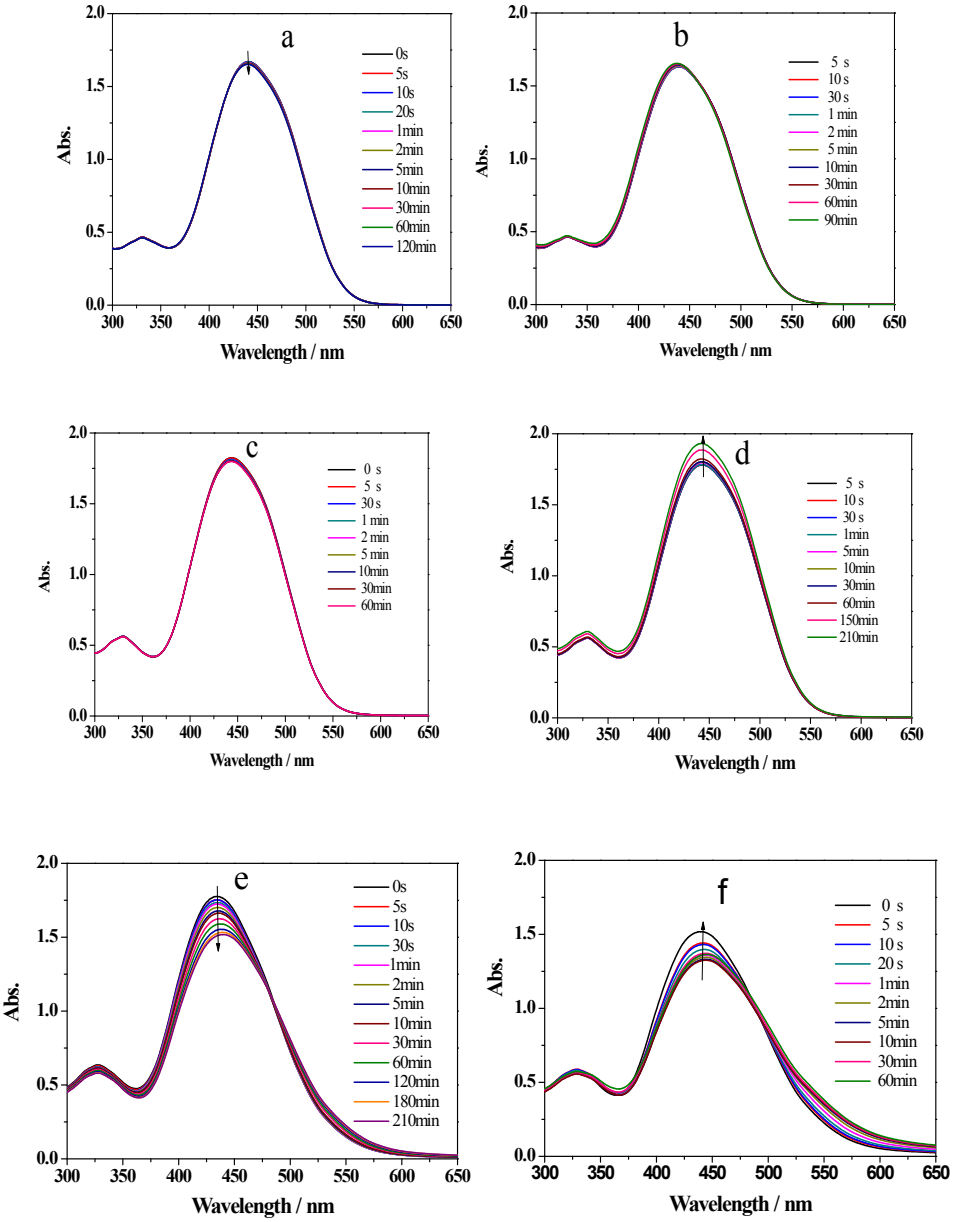


Figure S19. UV–Vis spectral change of Yb(**LB**)$_3$ in acetonitrile (a, b), ethanol (c, d) and hexane (e, f) ($2.0\times 10^{-5}$mol $L^{-1}$) solutions upon irradiation at 365 nm (a, c, e) and recoverable irradiation at 450 nm (b, d, f) as a function of time.

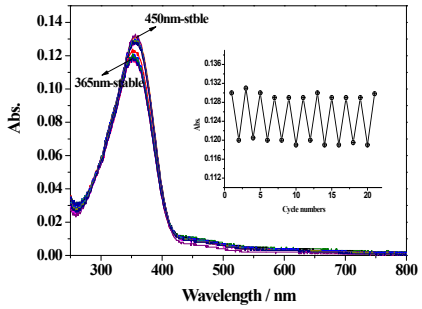


Figure S20. UV–Vis spectral change of La(**LA**)$_3$ in PMMA film (5.0wt%) upon irradiation at 365 nm and recoverable irradiation at 450 nm (Inset: reversible change of absorption intensity at 358 nm in the photostationary states after alternating irradiation at λ = 365 and λ = 450 nm in repeated switching cycles).

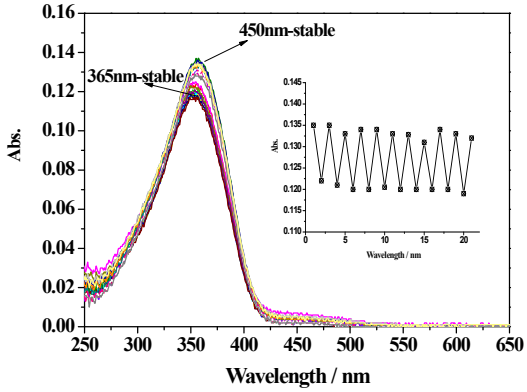


Figure S21. UV–Vis spectral change of Eu(**LA**)$_3$ in PMMA film (5.0wt%) upon irradiation at 365 nm (a) and recoverable irradiation at 450 nm (b) (Inset: reversible change of absorption intensity at 358 nm in the photostationary states after alternating irradiation at λ = 365 and λ = 450 nm in repeated switching cycles).

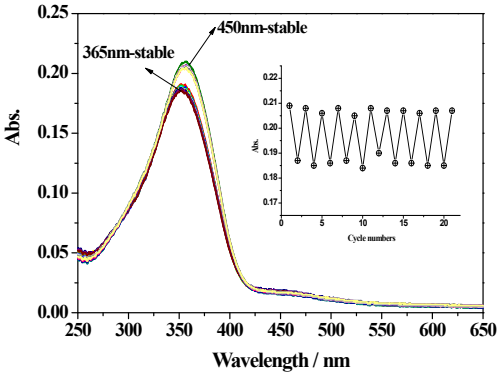


Figure S22. UV–Vis spectral change of Gd(**LA**)$_3$ in PMMA film (5.0wt%) upon irradiation at 365 nm (a) and recoverable irradiationat 450 nm (b) (Inset: reversible change of absorption intensity at 358 nm in the photostationary states after alternating irradiation at λ = 365 and λ = 450 nm in repeated switching cycles).

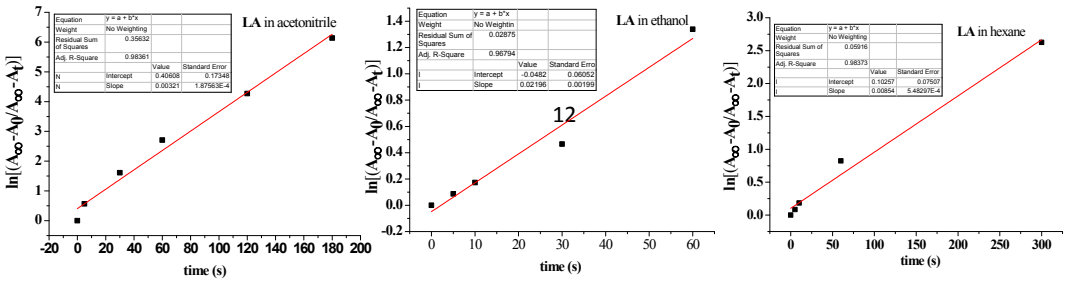

Figure S23. The *trans-cis* photoisomerization kinetics of ln(A∞−A$_0$)/(A∞−At) as a function of time for **LA** in different solvents.

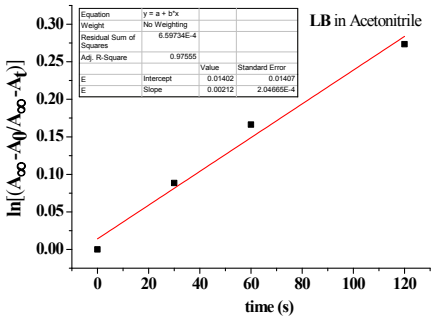


Figure S24. The *trans-cis* photoisomerization kinetics of ln(A∞−A$_0$)/(A∞−At) as a function of time for **LB** in acetonitrile.

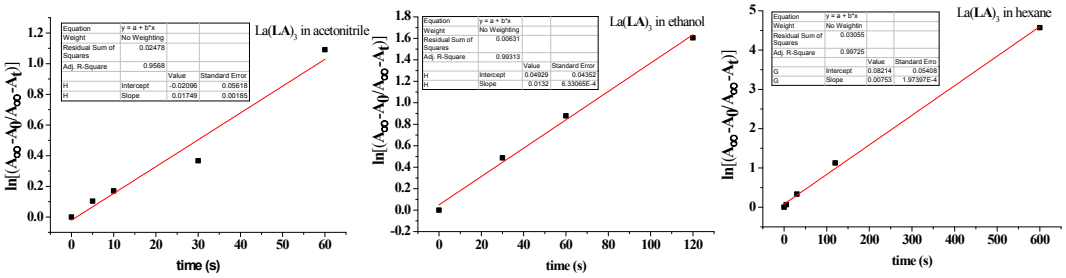


Figure S25. The *trans-cis* photoisomerization kinetics of ln(A∞−A$_0$)/( (A∞−At)) as a function of time for La(**LA**)$_3$ in different solvents.

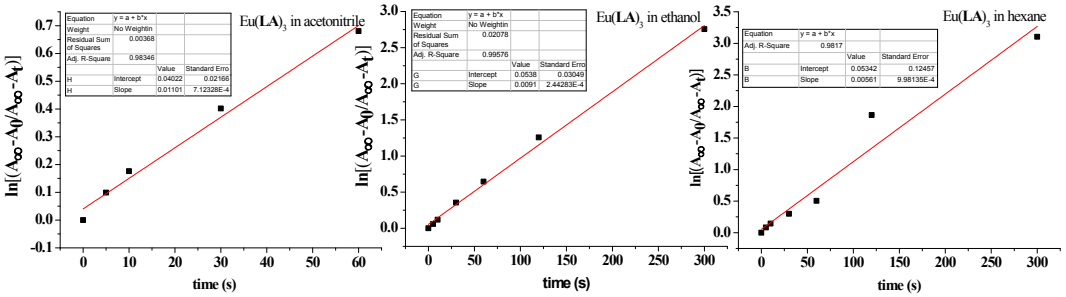


Figure S26. The *trans-cis* photoisomerization kinetics of ln(A∞−A$_0$)/( (A∞−At)) as a function of time for Eu(**LA**)$_3$ in different solvents.

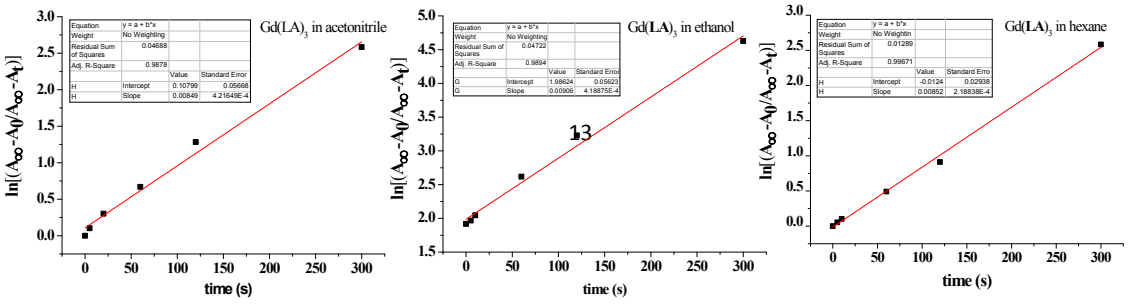

Figure S27. The *trans-cis* photoisomerization kinetics of ln(A∞−A$_0$)/( (A∞−At)) as a function of time for Gd(**LA**)$_3$ in different solvents.

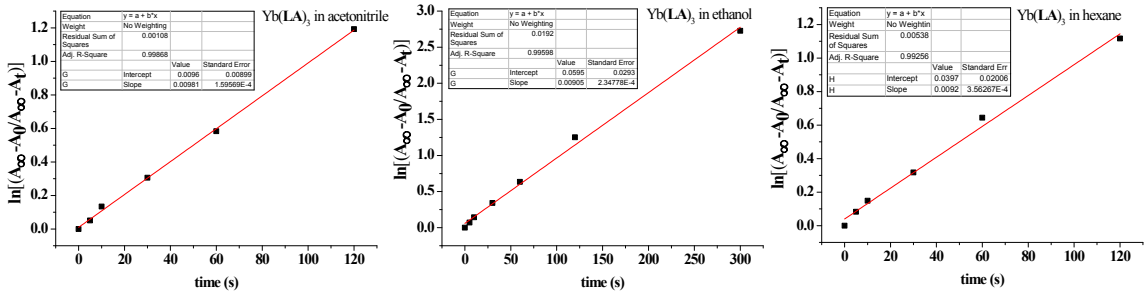


Figure S28. The *trans-cis* photoisomerization kinetics of ln(A∞−A$_0$)/( (A∞−At)) as a function of time for Yb(**LA**)$_3$ in different solvents.

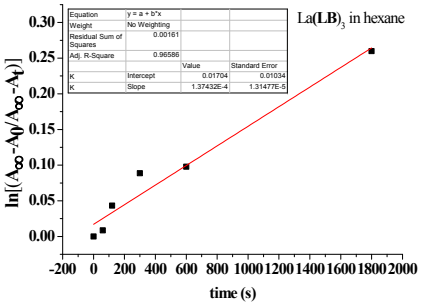


Figure S29. The *trans-cis* photoisomerization kinetics of ln(A∞−A$_0$)/( (A∞−At)) as a function of time for La(**LB**)$_3$ in hexane solution.

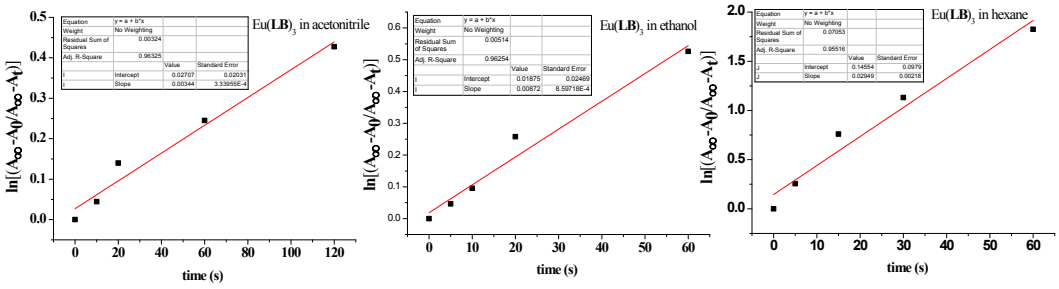


Figure S30. The *trans-cis* photoisomerization kinetics of ln(A∞−A$_0$)/( (A∞−At)) as a function of time for Eu(**LB**)$_3$ in different solvents.

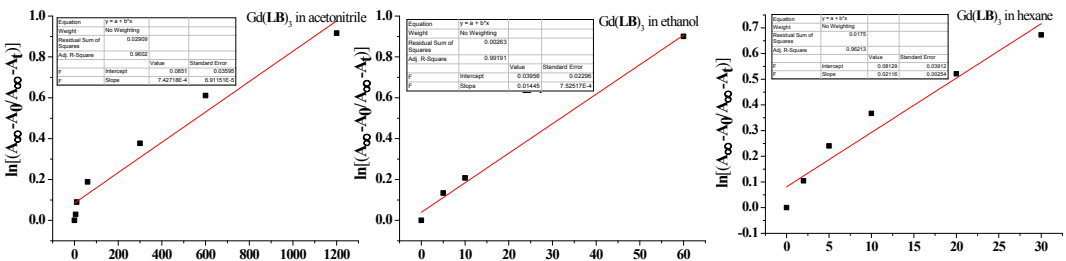

Figure S31. The *trans-cis* photoisomerization kinetics of ln(A∞−A$_0$)/( (A∞−At)) as a function of time for Gd(**LB**)$_3$ in different solvents.

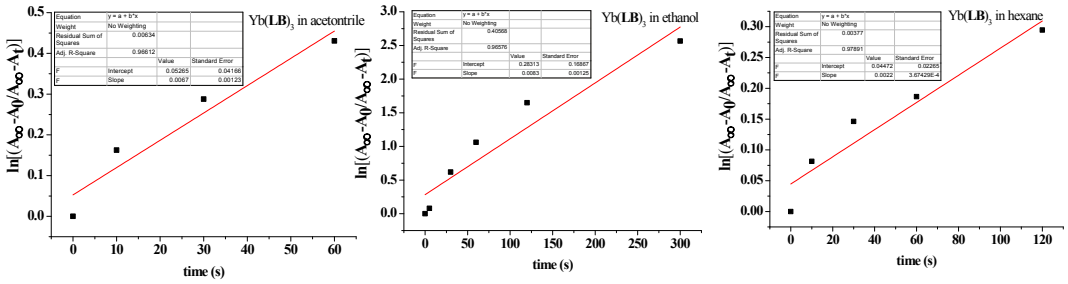


Figure S32. The *trans-cis* photoisomerization kinetics of ln(A∞−A$_0$)/( (A∞−At)) as a function of time for Yb(**LB**)$_3$ in different solvents.

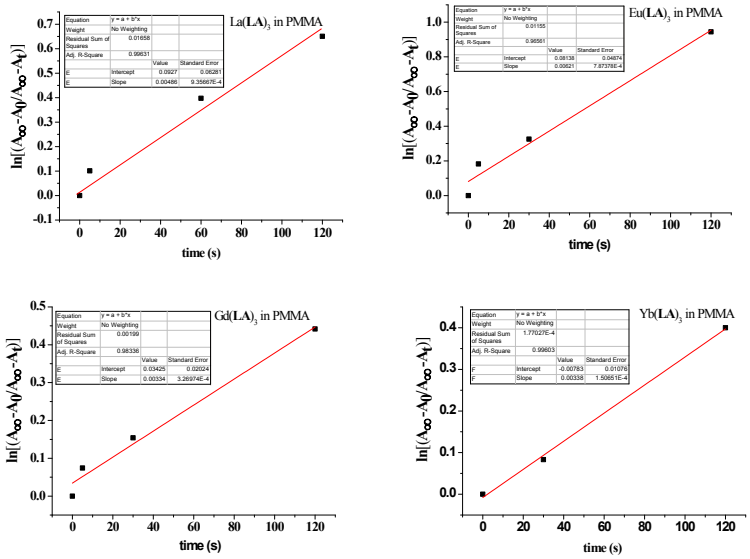


Figure S33. The *trans-cis* photoisomerization kinetics of ln(A∞−A$_0$)/( (A∞−At)) as a function of time for La(**LA**)$_3$, Eu(**LA**)$_3$, Gd(**LA**)$_3$ and Yb(**LA**)$_3$ in PMMA film.

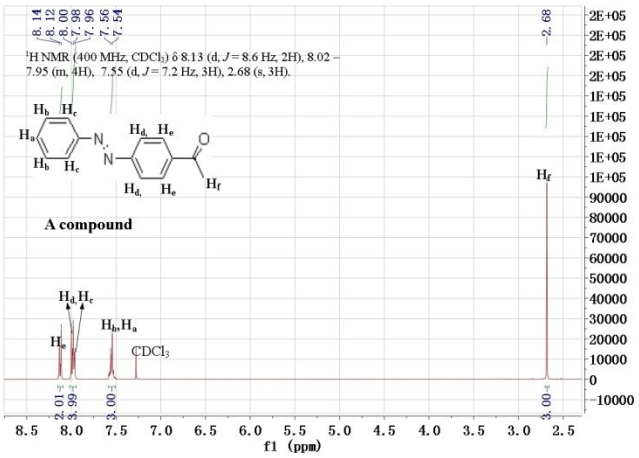


Figure S34. $^{1}$H NMR spectrum of **A** compound in $CDCl_3$.

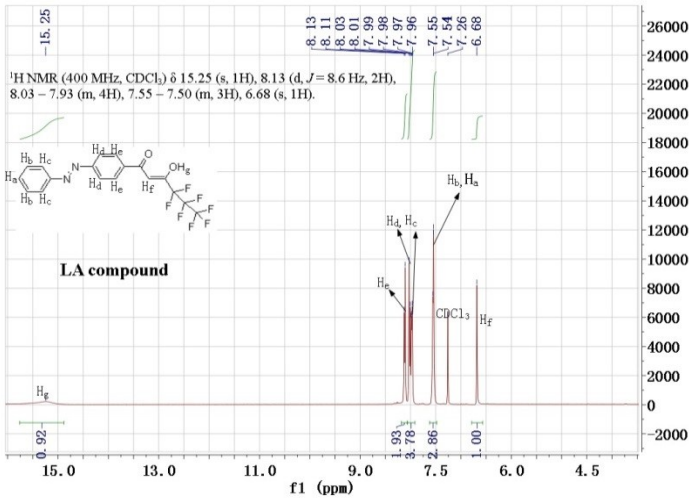


Figure S35. $^{1}$H NMR spectrum of **LA** ligand in $CDCl_3$.

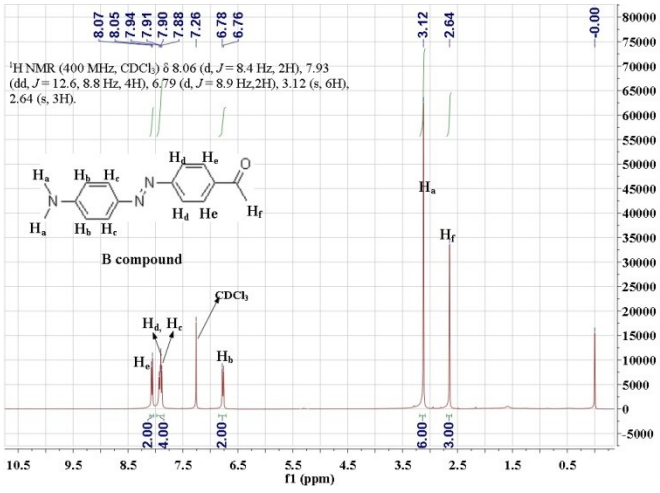


Figure S36. $^{1}$H NMR spectrum of **B** compound in $CDCl_3$.

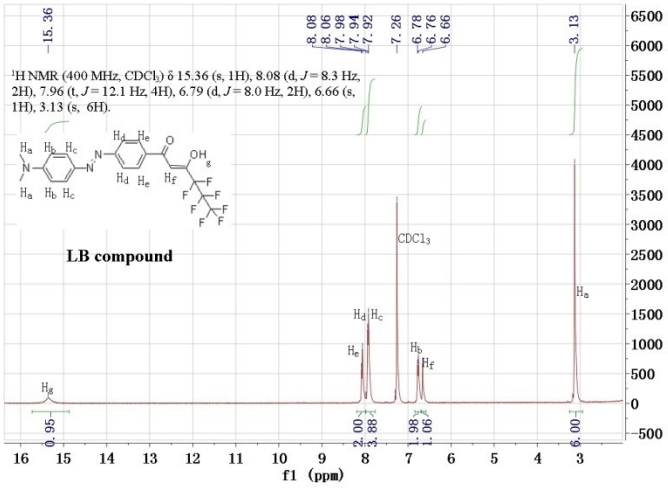


Figure S37. $^{1}$H NMR spectrum of **LB** ligand in $CDCl_3$.

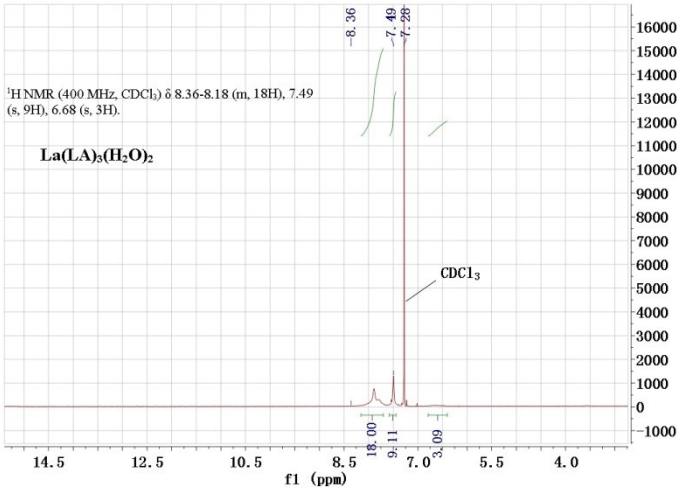


Figure S38. $^{1}$H NMR spectrum of complex La(**LA**)$_3$ in $CDCl_3$.

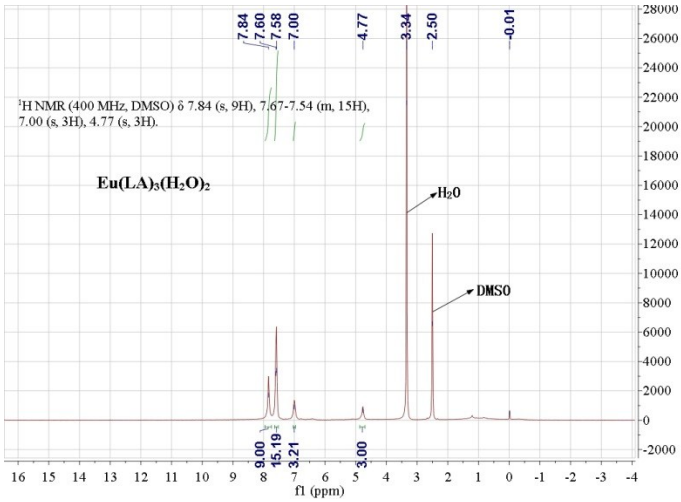


Figure S39. $^{1}$H NMR spectrum of complex Eu(**LA**)$_3$ in DMSO-$d_6$.

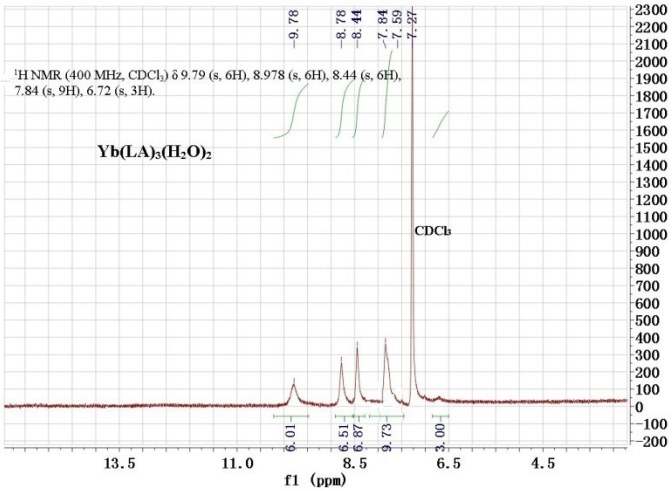


Figure S40. $^{1}$H NMR spectrum of complex Yb(**LA**)$_3$ in $CDCl_3$.

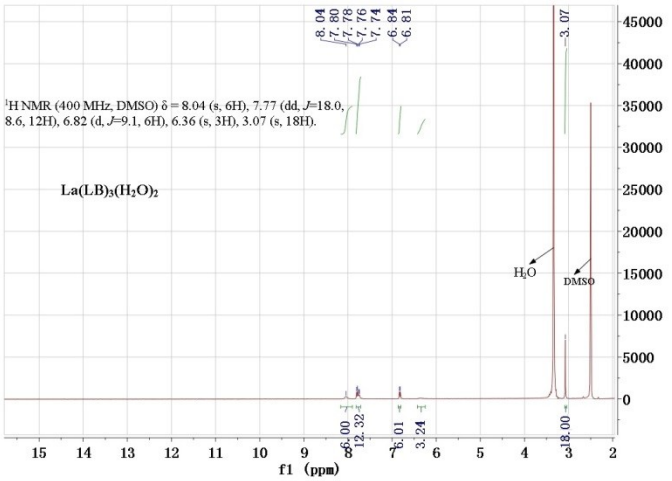


Figure S41. $^{1}$H NMR spectrum of complex La(**LB**)$_3$ in DMSO-$d_6$.

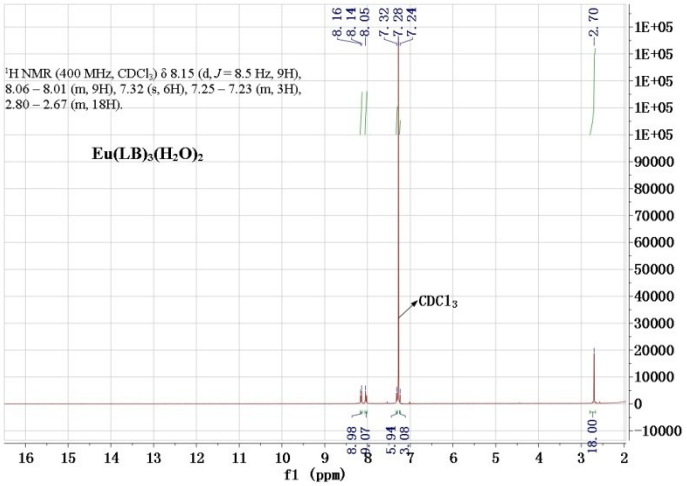


Figure S42. $^1$H NMR spectrum of complex Eu(**LB**)$_3$ in $CDCl_3$.

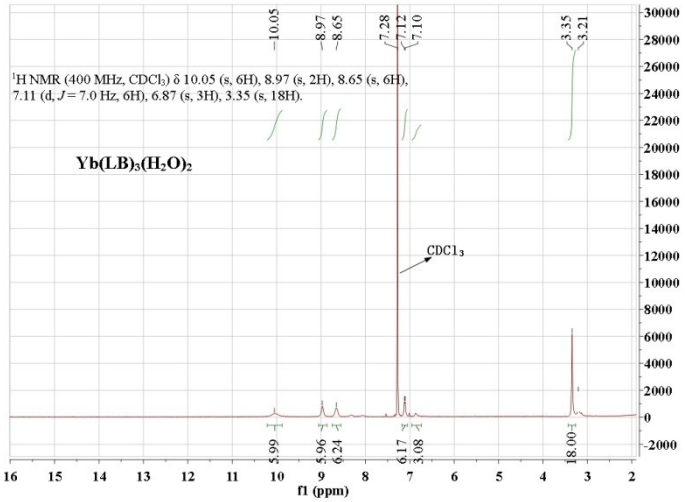


Figure S43. $^1$H NMR spectrum of complex Yb(**LB**)$_3$ in $CDCl_3$.

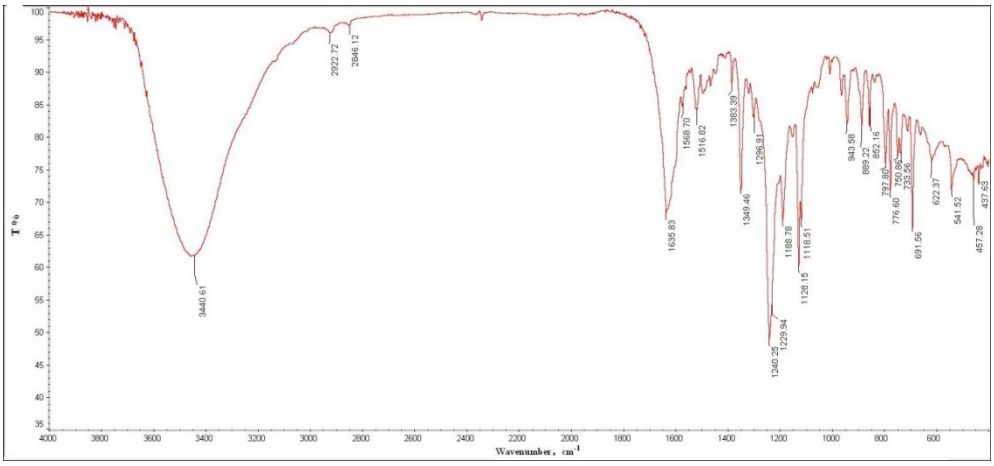


Figure S44. IR spectrum of **LA** ligand in KBr pellet.

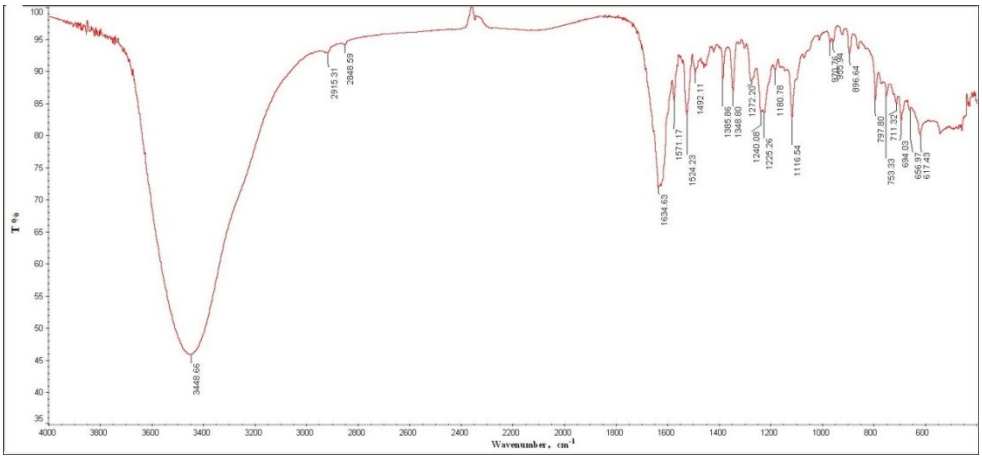


Figure S45 IR spectrum of complex La(**LA**)$_3$ in KBr pellet.

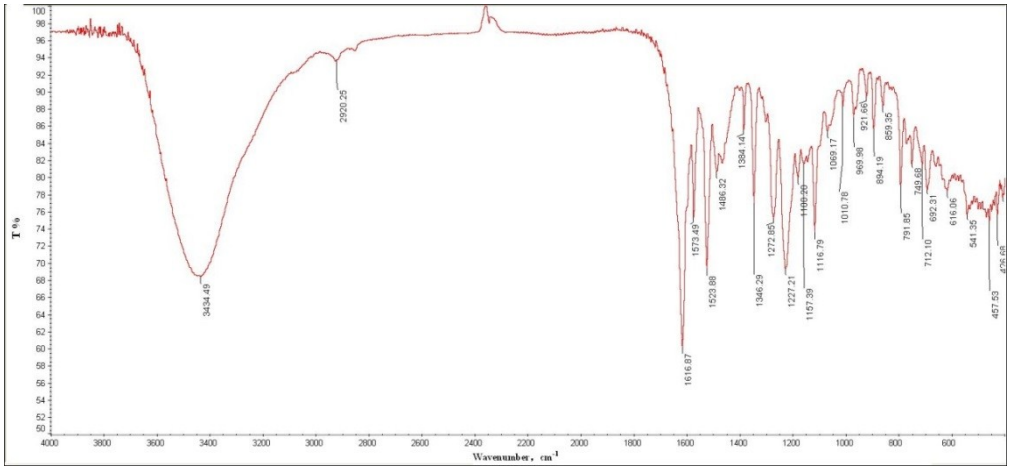


Figure S46. IR spectrum of complex Eu(**LA**)$_3$ in KBr pellet.

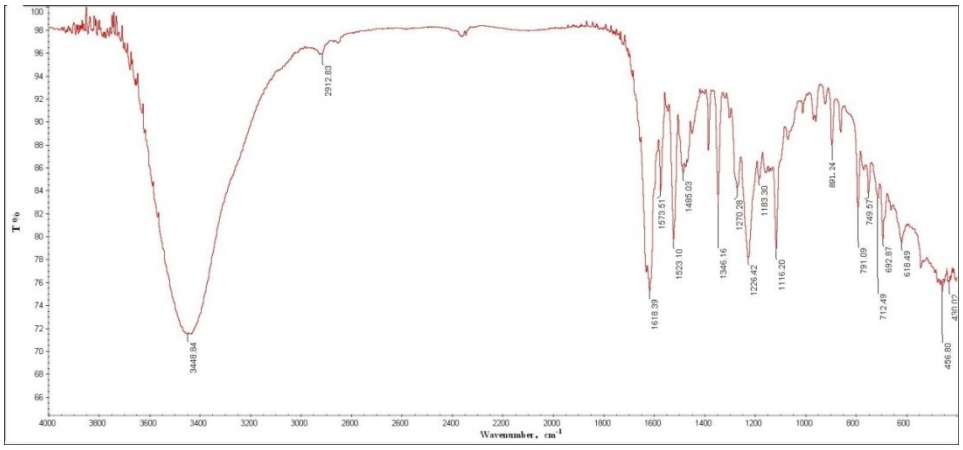


Figure S47. IR spectrum of complex Gd(**LA**)$_3$ in KBr pellet.

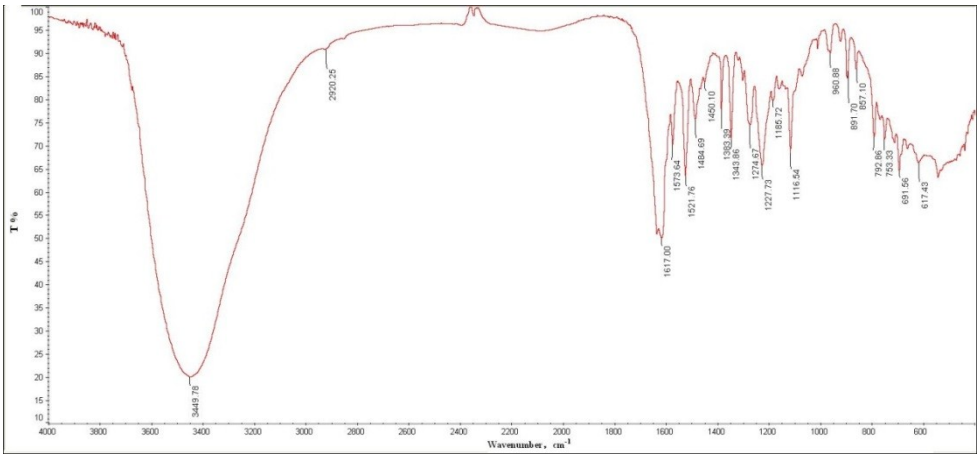


Figure S48. IR spectrum of complex Yb(**LA**)$_3$ in KBr pellet.

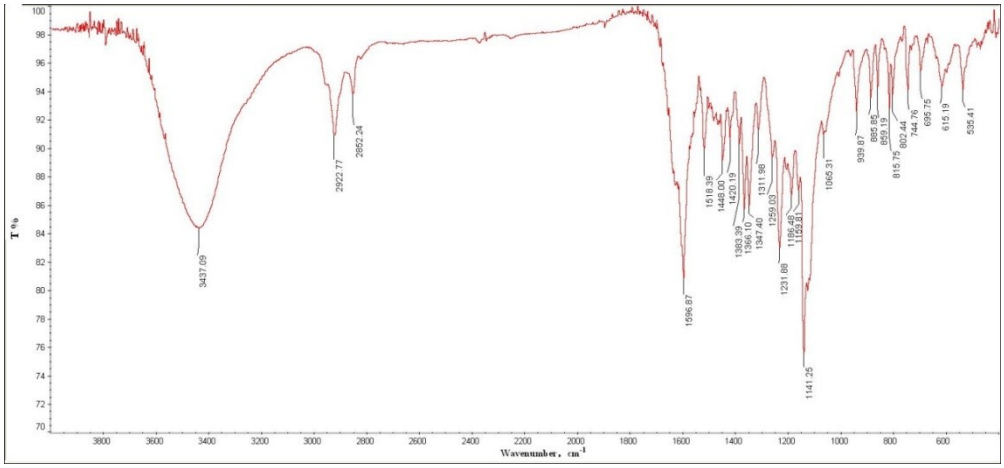


Figure S49. IR spectrum of complex **LB** ligand in KBr pellet.

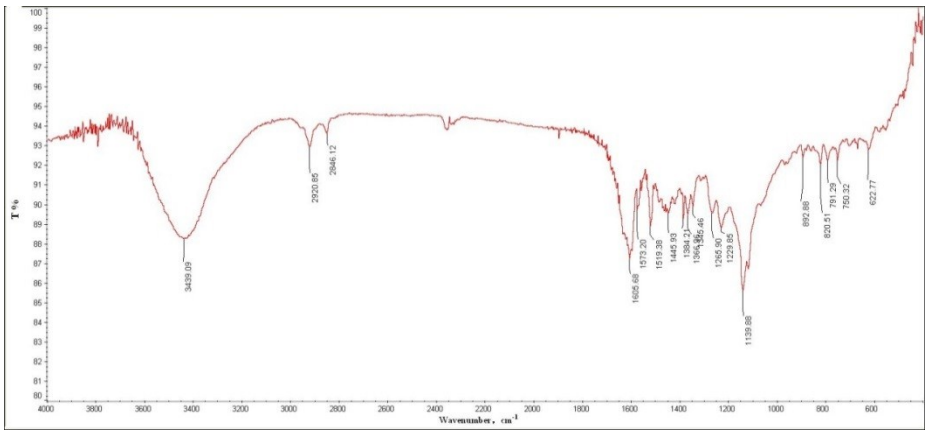


Figure S50. IR spectrum of complex La(**LB**)$_3$ in KBr pellet.

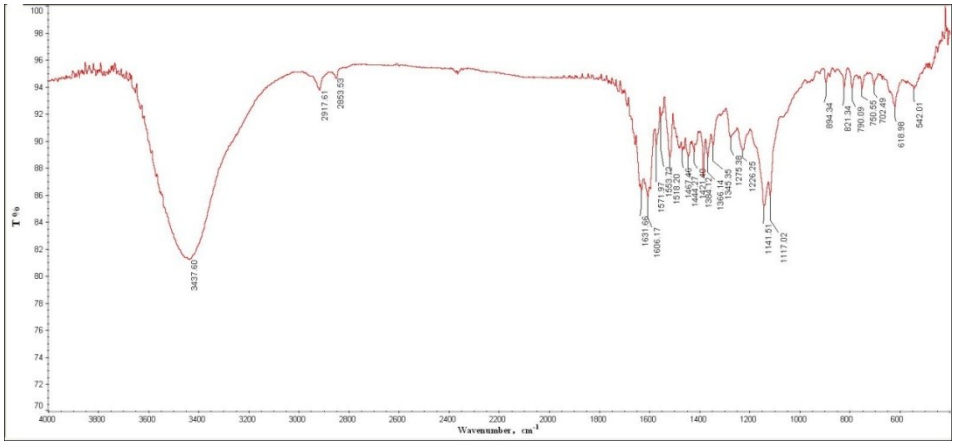


Figure S51. IR spectrum of complex Eu(**LB**)$_3$ in KBr pellet.

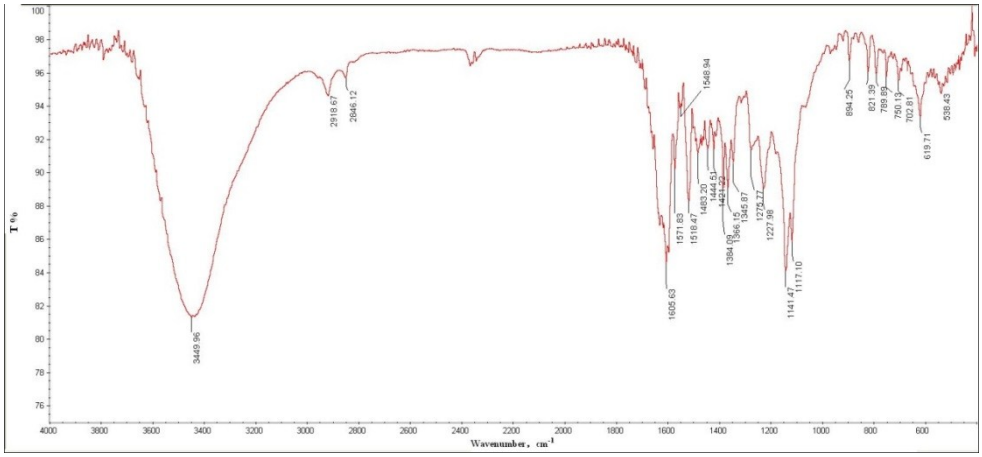


Figure S52. IR spectrum of complex Gd(**LB**)$_3$ in KBr pellet.

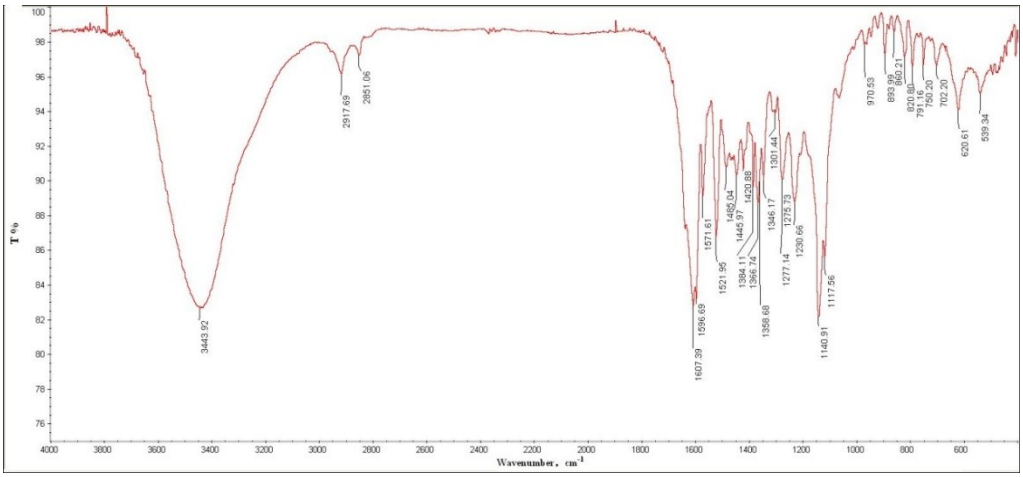


Figure S53. IR spectrum of complex Yb(**LB**)$_3$ in KBr pellet.